Applied Catalysis B: Environmental 188 (2016) 367–375

Contents lists available at ScienceDirect

Applied Catalysis B: Environmental

journal homepage: www.elsevier.com/locate/apcatb

Characterization and evaluation of Pt-Pd electrocatalysts prepared by electroless deposition

Akkarat Wongkaew[a,b], Yunya Zhang[b], John Meynard M. Tengco[b], Douglas A. Blom[b], PremKumar Sivasubramanian[c], Paul T. Fanson[c], John R. Regalbuto[b], John R. Monnier[b,*]

[a] Department of Chemical Engineering, Faculty of Engineering, Burapha University, Chonburi 20131, Thailand
[b] Department of Chemical Engineering, Swearingen Engineering Center, University of South Carolina, Columbia, SC 29208, United States
[c] Toyota Research Institute of North America, Ann Arbor, MI 48105, United States

ARTICLE INFO

Article history:
Received 16 October 2015
Received in revised form 19 January 2016
Accepted 7 February 2016
Available online 10 February 2016

Keywords:
Electroless deposition
Pt-Pd/C
Core-shell structures
PEM fuel cells
Bimetallic catalysts

ABSTRACT

Semi-continuous electroless deposition (ED) methods have been developed for preparation of variable and controlled coverages of Pt on Pd surfaces. The deposition of Pt occurred in an aqueous bath containing a reducible metal salt ($PtCl_6^{2-}$), reducing agent (hydrazine) and stabilizer (ethylenediamine). To avoid electrostatic adsorption of $PtCl_6^{2-}$, bath pH was controlled at pH 9.0, which was higher than the PZC of the carbon support, to create a negatively-charged carbon surface. Bath stability was maintained by addition of ethylenediamine and limiting the concentration of N_2H_4 in the bath to prevent thermal reduction of $PtCl_6^{2-}$ to form Pt^0. The concentration of N_2H_4 was controlled by pumping N_2H_4 solutions at various pumping rates into the ED bath. Thus, bimetallic Pt-Pd particles with Pt loadings of 6.0, 11.7, 17.2, and 22.7 wt% were selectively deposited on Pd surfaces of 30 wt% Pd/C. The structures of the catalysts were determined by STEM and EDS as variable thickness Pt shells with Pd cores. Pt loadings of 6.0, 11.7, 17.2, and 22.7 wt% corresponded to Pt shells of 0.9, 1.7, 2.7, and 3.4 monolayers (ML) on Pd. The catalysts were evaluated for their oxygen reduction reaction activity. The core-shell Pd-Pt/C catalysts were very active, especially the sample containing 0.9 ML Pt coverage on Pd with a mass activity of 329 A/g Pt compared to 183 A/g Pt for a conventional 50.5 wt% Pt/C sample. Similarly, electrochemical surface areas (ECSA) for all Pt shell samples (72–211 m^2Pt/g Pt) were higher than for the conventional catalyst (58 m^2Pt/g Pt).

1. Introduction

In order to achieve more environmentally-friendly energy sources, an electrically-based power system is critical. For stationary systems, alternatives such as wind, hydrothermal, and solar options are feasible. However, for mobile systems, fuel cells provide one of the most attractive options, and of these, hydrogen (PEM) fuel cells are the most amenable for transportation power [1]. Pt is considered to be the preferred metal catalyst in proton exchange membrane fuel cell (PEMFC) applications because of a unique set of advantages for use in vehicles: a sufficiently low working temperature (80 °C), a good energy density versus other fuel cell types, robust and relatively simple design, and perhaps most importantly, its stability in the acidic and corrosive oxygen reduction reaction (ORR) environment [1]. However, to achieve adequate current densities, contemporary PEMFCs use very high weight loadings of Pt supported on conductive carbon supports, particularly for the relatively slow ORR; Pt loadings as high as 60–80 wt% have sometimes been used to achieve acceptable levels of performance [2–5]. For example, Gasteiger et al. [5] has reported that Pt weight loadings of 40–50 wt% Pt on carbon support were needed to achieve acceptable performance levels. However, due to its high cost, Pt content has a great impact on the cost of mass production of PEMFCs. Thus, much of current research involves design of catalysts where Pt is used more efficiently. One of the obvious considerations is to use Pt only as a thin shell over a less expensive core metal such as Co, Ni, Ru, or even Pd [6–12]. Since catalysis and the ORR reaction is a surface phenomenon [1,4], in principle a single monolayer (ML) thickness represents the most efficient use of Pt. In addition to the more efficient use of Pt, a thin Pt shell layer can also interact electronically with the metal core to increase ORR activity by either compression of the Pt–Pt bond distance at the interface and near-interface layers of the core and Pt shell and/or by an increase in the Pt 3d orbital vacancies [13,14]. Finally, the formation of a complete core-shell structure may also retard the dissolution of the metal

* Corresponding author.
E-mail address: monnier@cec.sc.edu (J.R. Monnier).

http://dx.doi.org/10.1016/j.apcatb.2016.02.022
0926-3373/

core at the strong acidic conditions of the cathode during PEMFC operation and prevent the Pt shell from sintering [14,15].

Thus, much effort is devoted to developing preparative methods that ensure formation of controlled-thickness shells of Pt over metal cores. Conventional catalyst preparation methods of wet impregnation and incipient wetness are not well-suited for formation of bimetallic core-shell compositions [16]. Co-impregnation or successive impregnation of two different metal salts typically form monometallic particles of each metal as well as variable-composition bimetallic particles with little discrimination between bulk and surface metal atoms. Other approaches have included electrochemical or galvanic displacement [17–20], solvothermal methods [21], successive reduction [22], reduction-precipitation [23], dc magnetron co-sputtering [24], one-step ultraviolet irradiation [25], reverse microemulsion [26], microwave heating [27], molecular beam epitaxy [28], and mechanical alloying methods [29]. An alternative method that offers potential for core-shell structures is electroless deposition (ED) [10–12,30–33]. ED is a catalytic or autocatalytic process whereby a shell of controllable thickness or a partial shell of metal can be deposited selectively onto pre-existing core particles (or seed nuclei) of a pre-existing metal. In principle, there is no formation of isolated crystallites of the second metal on the catalyst support [34]. We have previously prepared bimetallic Pt core-shell materials such as Pt-Pd/C, Pt-Rh/C and Pt-Co/C as catalysts for PEMFC applications [11,12,31]. In these studies, potassium hexachloroplatinate (K_2PtCl_6) and dimethylamine borane (DMAB) were used as the Pt salt and reducing agent, respectively. Sodium citrate was used to stabilize $PtCl_6^{2-}$ from thermal or spontaneous reduction to form Pt^0 particles in the ED bath before electroless deposition could occur. Scanning transmission electron microscopy (STEM) and energy dispersive X-ray analysis (EDS) confirmed that bimetallic core-shell structures were formed when sufficient Pt was deposited on the Pd, Rh, and Co cores. However, in most cases, the Pt loadings were intentionally restricted to less than one monolayer of Pt coverage since the goal was to prepare bimetallic surfaces. In those cases where multiple layers of Pt were deposited, characterization and evaluation as ORR catalysts were limited. Finally, the amounts of core-shell catalysts prepared were small enough (<2–3 g) so that batch methods of ED were used.

In this study, we extend our earlier work on the electrochemical and structural characterization of Pd@Pt/C (Pt deposited on Pd cores) catalysts prepared by ED. Platinum shell thicknesses have been systematically varied from approximately 1–3 monolayers on a 30 wt% Pd/C base catalyst. Because of the relatively large amounts of Pt deposited on the high weight loading Pd/C catalyst, we have developed a semi-continuous method of ED; the hydrazine (N_2H_4) reducing agent solution is pumped continuously into a vessel containing the H_2PtCl_6 and ethylenediamine aqueous solution and a slurry of the 30 wt% Pd/C catalyst. The amounts of Pt deposited on the Pd core particles have been determined by controlling the amounts of H_2PtCl_6 salt initially in solution. In addition to characterization by STEM and EDS, chemisorption by H_2 was also used to determine the concentration of Pt plus Pd surface sites, from which inferences concerning the specificity of Pt deposition only on Pd cores could be made.

2. Experimental

2.1. Catalyst preparation

The 30 wt% Pd/C monometallic base catalyst was a high Pd loading catalyst provided by Toyota Motor Company. The concentration of Pd surface sites was determined by H_2 titration of oxygen precovered Pd sites (Pd-O) using a Micromeritics Autochem II 2920 automated chemisorption analyzer. The different ML coverages of Pt on the Pd core were also analyzed by H_2 titration of oxygen precovered Pt along with residual, exposed Pd sites from incomplete coverage by Pt, since both Pd and Pt have similar chemisorption behavior [35]. Before H_2 titration, samples were pretreated *in situ* for 2 h at 200 °C in flowing 10% H_2/balance Ar before O_2 exposure and H_2 titration at 40 °C were conducted. Details of this procedure have been discussed in previous work [36]. Hydrogen titration results for 30 wt% Pd/C gave 2.09×10^{20} surface Pd sites/g cat for a dispersion of 12.5% corresponding to average Pd particle diameters of 4.5 nm. The value of 2.09×10^{20} Pd sites/g cat was used for calculation of Pt deposition to give one theoretical monolayer of Pt, assuming monodisperse deposition of Pt.

Bimetallic compositions were prepared using a semi-continuous method of electroless deposition, rather than the batch method (all components initially present in the ED bath) used in previous efforts [10–12,30–33] where the goal was to prepare fractional coverages of the ED metal. The concentrations of hydrazine (N_2H_4) reducing agent and chloroplatinic acid (H_2PtCl_6) required for even a single monolayer coverage of Pt (6.2 wt% Pt) on 30 wt% Pd/C were so high that thermal stability of the bath, even using ethylenediamine (EN) as a chelating and stabilizing agent, was not attainable, in agreement with observations of others [37,38]. Thus, the ED bath initially contained the desired concentration of H_2PtCl_6 (Sigma-Aldrich), EN (Sigma-Aldrich), 30 wt% Pd/C catalyst, and deionized water adjusted to pH 9.0; at pH 9.0, H_2PtCl_6 existed as $PtCl_6^{2-}$ in solution. The volume of this bath was 150 mL. Unless otherwise stated, the molar ratio of [EN]/[$PtCl_6^{2-}$] was maintained at 2/1. The required amount of N_2H_4 to give final molar ratios of [N_2H_4]/[$PtCl_6^{2-}$]/[EN] = 5/1/2 was dissolved in 50 mL of deionized water (pH 9.0) and loaded into a 60 mL syringe and placed in a microprocessor-controlled syringe pump (NE-1000 Programmable Single Syringe Pump). The N_2H_4 solution was pumped into the well-stirred ED bath at different pump rates (1.67 mL/min, 1.25 mL/min, 1.11 mL/min, 1.00 mL/min, 0.50 mL/min and 0.20 mL/min); the total volume of the ED bath containing all components was 200 mL. The total deposition period was 1 h, even though at the highest pump rate of 1.67 mL/min N_2H_4 addition was completed after 30 min while for a pump rate of 0.20 mL/min only 12 mL of N_2H_4 solution had been added. During the period of ED, the pH of the ED bath was maintained between 9.0–10.0 using a standard NaOH solution and ED bath temperature was controlled at 30 °C.

To measure the kinetics of $PtCl_6^{2-}$ deposition, <1 mL aliquots of liquid were collected and filtered using 2 μm mesh syringe filters at various time intervals to monitor the time-dependent concentrations of $PtCl_6^{2-}$ remaining in the ED bath. The collected liquid samples were analyzed for $PtCl_6^{2-}$ concentrations by either of two analytical tools, ICP-OES spectroscopy (Optima DV 2000 Perkin-Elmer) or UV–vis absorption spectroscopy (UV–1800 Shimadzu). After the completion of ED, the solutions were filtered and the catalysts were washed thoroughly with 3 L of 18.2 MΩ-cm deionized water (Thermo Scientific Barnstead Nanopure Ultrapure Water System) to remove all soluble ions and salts. Samples were dried *in vacuo* at room temperature and stored at ambient conditions.

2.2. Catalyst characterization

Scanning transmission electron microscopy (STEM) was used to image the structure of the Pt shell-Pd core compositions using a JEOL 2100F 200 kV FEG-STEM/TEM equipped with a CEOS Cs corrector on the illumination system. The geometrical aberrations were measured and controlled to provide less than a π/4 phase shift of the incoming electron wave over the probe-defining aperture of 17.5 mrad which at 200 kV provides a nominal probe size of <0.1 nm. High angle annular dark-field (HAADF) STEM images were acquired on a Fischione Model 3000 HAADF detector with a camera

length such that the detector spanned 50–284 mrad. The scanning acquisition was synchronized to the 60 Hz AC electrical power to minimize 60 Hz noise in the images and a pixel dwell time of 15.8 μs was chosen. Energy dispersive spectral (EDS) images were acquired with a 100 pA probe produced by a probe-defining aperture of 24 mrad. Pixel dwell time for the EDS data was 4 s. Drift correction of the EDS data acquisition was performed as implemented in the Digital Micrograph software of Gatan Inc.

2.3. Catalyst evaluation

Electrochemical evaluation was performed in a conventional three-electrode cell using the ring disk electrode (RDE) technique. A glassy carbon disk with an area of 0.196 cm^2 was coated with thin film of catalysts to form a working electrode. The catalyst ink was prepared by ultrasonically and mechanically stirring at room temperature a mixture of catalyst, ethanol and Nafion 117 solution; the concentration of Nafion was 5% in a mixture of 2-propanol, *n*-propanol and water to give a final composition of 5% Nafion, 45% H_2O, and 50% alcohols. Ten μL of catalyst ink was pipetted onto the glassy carbon disk surface with a carbon loading of 13.6 μg/cm^2. After air drying, a catalyst film was formed. This working electrode was transferred to the electrochemical cell for measurements. The electrochemical cell consisted of a five necked flask with a mercury sulfate electrode as a reference electrode and a platinum wire as a counter-electrode. The electrolyte was 0.1 M $HClO_4$; electrochemical measurements were conducted at 27 °C and the working electrode was immersed in the electrolyte. Before electrochemical evaluations the electrode surface was preconditioned by cycling at 500 mV/s. Cyclic voltammetry (CV) was measured in the electrolyte saturated with N_2 with the potential sweeping between 0.05 and 1.20 V at 50 mV/s. For ORR activity measurements, linear sweep voltammetry (LSV) was conducted between 1.2 V and 0.05 V vs SHE at 10 mV/s at rotation speeds of 400, 900, 1600 and 2500 rpm in the O_2-saturated electrolyte. The electrochemical surface area (ECSA) and mass activity of the catalyst (MA) were calculated from the CV and ORR activity results.

3. Results and discussion

3.1. Strong electrostatic adsorption and thermal decomposition

In general, ED baths contain a reducible metal salt, reducing agent, and solvent (typically water at a particular pH). The ED bath is thermodynamically unstable, but kinetically stable in the absence of a catalyst. Kinetic stability is defined as the length of time required to complete the electroless deposition of the reducible metal salt, typically on the order of ≤2 h for most ED baths [39]. However, in this study kinetic stability of 20 min was sufficient to permit complete deposition of the reducible $PtCl_6^{2-}$ salt. In order to maintain bath stability, various chemical additives such as stabilizers, promoters or inhibitors can be added to the bath [39,40]. Further, electrostatic adsorption of the reducible metal salt on the catalyst support must be avoided by proper selection of the reducible metal salt such that the electrostatic charge of the catalyst support and the reducible metal salt component are the same. Since typical reducing agents are most effective at basic pH conditions, the pH of the ED bath must be maintained above the point of zero charge (PZC) of the catalyst support. The PZC of the carbon support in this study was measured to be pH 3.4 using the method described by Regalbuto [41]; thus, anions of the reducible metal salt must be used and this study, $PtCl_6^{2-}$ was selected. To determine its concentration in the ED bath, either ICP or UV–vis spectroscopy was used; both analytical methods gave similar results. Initially, the stability of $PtCl_6^{2-}$ at pH 9.0 was determined and aliquots of the

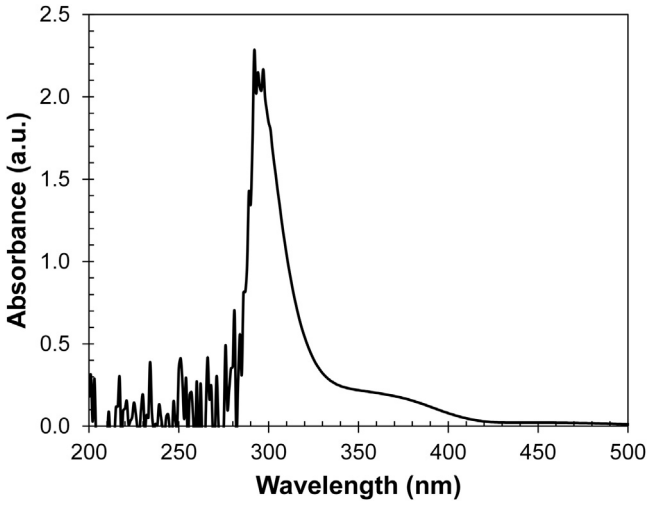

Fig. 1. UV–vis spectra of $PtCl_6^{2-}$ in water at pH 9.0. The above spectrum is actually six different spectra, all superimposed on each other, to indicate stability of $PtCl_6^{2-}$.

$PtCl_6^{2-}$ solution were measured at 10 min intervals for 1 h. Using UV–vis spectroscopy, the results in Fig. 1 indicate, there were no discernable changes in the spectra and that $PtCl_6^{2-}$ did not undergo hydrolysis at these conditions. The UV–vis spectra of $PtCl_6^{2-}$ in Fig. 1 shows three bands, a high intensity band at 294 nm corresponding to ligand to Pt charge transfer, diagnostically characteristic of the $PtCl_6^{2-}$ complex, and two broad, weak bands at 370 nm and 480 nm, both attributed to d–d orbital transitions of the complex [42,43]. The absorbance at 480 nm in Fig. 1 is especially weak and broad at these concentrations, but is diagnostic as one of the three bands for $PtCl_6^{2-}$. The intensity of the band at 294 nm was correlated to $PtCl_6^{2-}$ concentration, particularly to $PtCl_6^{2-}$ remaining in the ED bath.

In our previous work [9,12], the deposition of Pt on Pd/C was restricted to approximately one monolayer of Pt on 0.5–5.0 wt% Pd/C base catalysts. For these bimetallic catalysts, dimethylamine borane (DMAB) was used as the reducing agent. However, for multilayer loadings of Pt on high loadings of Pd/C, the concentrations of reducing agent and $PtCl_6^{2-}$ are necessarily very high. This leads not only to thermal instability of the ED bath but also potential contamination by organic residues from oxidation of DMAB on the catalyst surface during ED, which can lead to fouling [41] and no further deposition of Pt on active sites. Thus, a reducing agent such as N_2H_4 that contains no organic by-products (only gas phase products) from oxidation is preferred. The standard oxidation potential at basic conditions for N_2H_4 is given as:

$$N_2H_4 + 4OH^- \rightarrow N_2 + 4H_2 + 4e^-, \quad E^o = 1.16V$$

Because N_2H_4 is a strong reducing agent, the batch ED mode is not feasible, since bath stability is a strong function of N_2H_4 concentration. To prevent thermal reduction of $PtCl_6^{2-}$, N_2H_4 concentrations must be controlled. One way to achieve this is to pump N_2H_4 into the ED bath, denoted as semi-continuous ED, since all $PtCl_6^{2-}$ is initially added to the ED bath.

Before ED of Pt on Pd/C, the ED bath stability was determined by syringe-pumping 50 mL of a 1.39×10^{-2} M N_2H_4 solution into an ED bath containing $PtCl_6^{2-}$ in water at pH 9.0. The pumping rate was 1.67 mL/min and the initial concentration of $PtCl_6^{2-}$ in the bath was 6.96×10^{-4} M. After 30 min of pumping, the final $[N_2H_4]/[PtCl_6^{2-}]$ ratio was 5/1, assuming no reaction. The disappearance of $PtCl_6^{2-}$ in the bath (due to formation of metallic Pt particles) was monitored by UV–vis spectroscopy. The time dependent UV–vis spectra are shown in Fig. 2. In Fig. 2a, the absorbance intensity at 294 nm decreased with time and the bath became completely unstable,

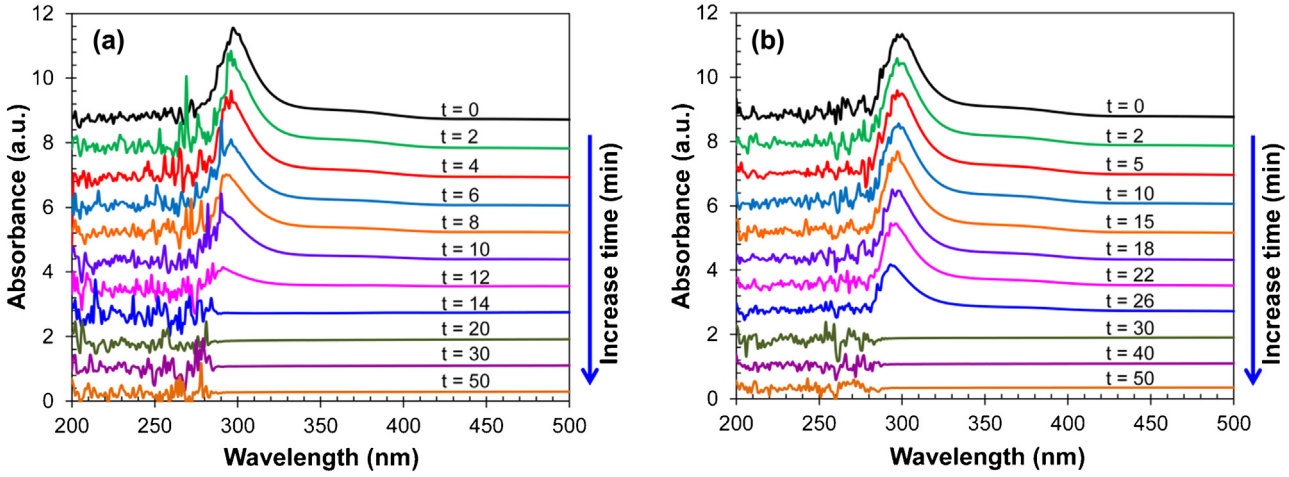

Fig. 2. Time dependent UV–vis spectra at 30 °C for bath stability tests (a) without addition of stabilizer: $[N_2H_4]/[PtCl_6^{2-}] = 5/1$ and (b) with the addition of stabilizer: $[N_2H_4]/[PtCl_6^{2-}]/[EN] = 5/1/2$.

forming visible, dark gray Pt particles after 12 min of exposure, when less than half of the N_2H_4 had been added. Thus, in order to maintain the bath stability, a stabilizer is required. In the subsequent experiment, ethylenediamine (EN) was added as a stabilizer since amines are good coordinating ligands and are readily removed during ED. Fig. 2b shows the time dependent UV–vis spectra of the ED bath containing $PtCl_6^{2-}$ and EN. The bath exhibited significantly greater stability and longer lifetime in the presence of EN; formation of Pt particles occurred rapidly only after 26 min, giving a stability enhancement of 14 min. Because absorbance peak widths were similar, peak heights of $PtCl_6^{2-}$ at 294 nm were linearly correlated with $PtCl_6^{2-}$ concentration remaining in the ED bath and the results are shown in Fig. 3. For the unstabilized ED bath, greater than 95% of $PtCl_6^{2-}$ was reduced to Pt^0 within 12 min, while the bath containing EN was fully stable for 15 min and gave good stability for approximately 25 min. In both cases, when the concentration of metallic Pt particles becomes high enough, there is a rapid transition from thermal to Pt-catalyzed reduction of $PtCl_6^{2-}$ and the concentration of $PtCl_6^{2-}$ rapidly declines to zero.

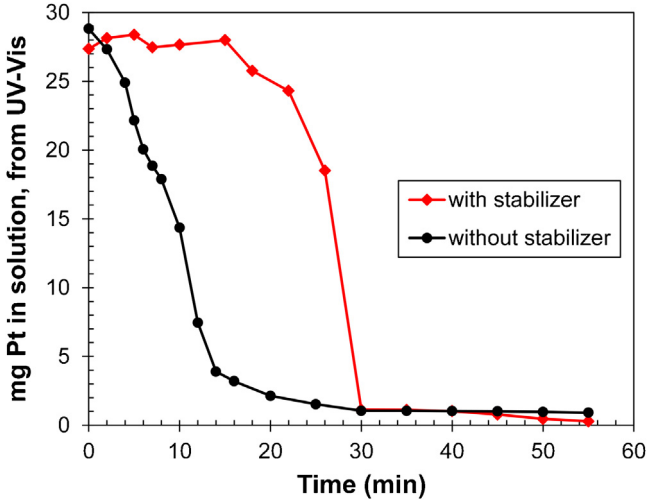

Fig. 3. Stability test from the ED bath with and without stabilizer at 30 °C using UV–vis absorbance to analyze Pt salt concentrations in solution. Y-axis displayed as mg Pt, although species in solution is $PtCl_6^{2-}$. Final ED bath composition if no reaction occurred was $[N_2H_4]/[PtCl_6^{2-}]/[EN] = 5/1/2$. Pumping speed of N_2H_4 solution (pH 9.0) was 1.67 mL/min for 30 min.

Because bath stability was controlled by N_2H_4 concentration, the effect of variable N_2H_4 pumping speeds was also determined and the results are shown in Fig. 4. The $PtCl_6^{2-}$ remaining in the bath as a function of time was analyzed by either ICP or UV–vis spectroscopy. Both analytical methods in general give similar curve shapes and stabilities, although more data points are obtained for the UV–vis mode of sampling and only $PtCl_6^{2-}$ is detected at 294 nm. At a pumping rate of 1.67 mL/min, the bath was stable for 25 min, while lowering the pump rate to 1.00 and 0.50 mL/min increased bath stability to approximately 40 and 70 min, respectively. The stability curves do appear slightly sharper for samples (at the edge of bulk instability) analyzed by ICP, although this is likely due to passage of the extremely small Pt^0 nuclei through the syringe filter in the very early stages of thermal reduction. This would mean that these small metal nuclei would be analyzed by ICP along with unreacted $PtCl_6^{2-}$ to give the mistaken appearance of added stability; UV–vis analyzes only the $PtCl_6^{2-}$ remaining in solution. For both methods stability drops rapidly due to transition from thermal to auto-catalytic deposition of $PtCl_6^{2-}$ by pre-existing Pt metal nuclei. These rapid kinetics of auto-catalytic deposition suggest that the thermal stabilities at all pump speeds should be sufficient for catalytic deposition to be completed before thermal reduction occurs.

3.2. Synthesis of Pt-Pd/C catalysts

Chemisorption results had previously indicated the concentration of surface Pd sites for 30 wt% Pd/C was 2.09×10^{20} surface Pd sites/g cat. For monodisperse coverage (Pt/Pd = 1) of Pt on Pd, 2.09×10^{20} Pt atoms/g cat, or 6.2 wt% Pt is required for 1 ML coverage. Fig. 5 shows the time-dependent profiles for ED of $PtCl_6^{2-}$ to give different coverages of Pt on the Pd surface. Note that higher coverages of Pt were accomplished by simply increasing the initial concentration of $PtCl_6^{2-}$ in the ED bath and adjusting the concentrations of N_2H_4 and EN accordingly.

For all $PtCl_6^{2-}$ concentrations, deposition was essentially completed after 20 min, even though only ~67% of the N_2H_4 had been added; however, at basic conditions N_2H_4 is considered to be a $4e^-$ reducing agent, assuming 100% selectivity. After 20 min of ED, the total amount of N_2H_4 added to the bath corresponded to an initial molar ratio of $[N_2H_4]/[PtCl_6^{2-}] = 3.3/1$; thus, ample N_2H_4 had been added, even after 20 min. In all cases, ED was completed within the timeframe of thermal stability of the ED bath and that controlled pumping of N_2H_4 into a bath containing initially high concentrations of $PtCl_6^{2-}$ was an effective method of depositing

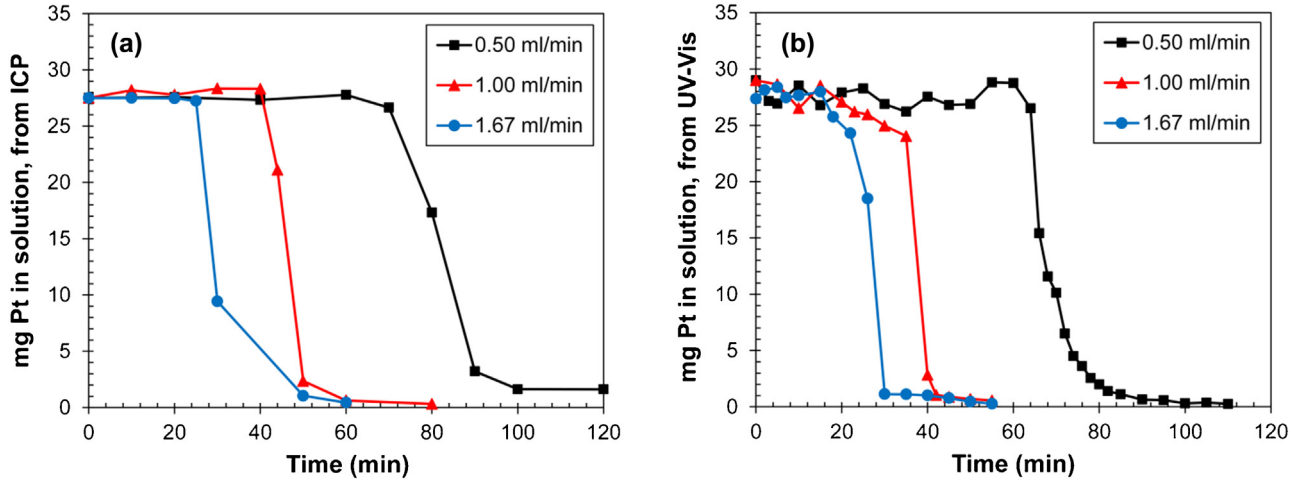

Fig. 4. Results of bath stability test for different pumping rates of N_2H_4 solution at 30 °C and final concentration of $[N_2H_4]/[PtCl_6^{2-}]/[EN] = 5/1/2$ (after pumping ceased). (a) Results based on ICP analysis of $PtCl_6^{2-}$. (b) Results based on UV–vis analysis. (■) 0.50 cc/min for 100 min, (▲) 1.00 mL/min for 50 min, and (●) 1.67 mL/min for 30 min.

multiple layers of Pt over Pd cores. Characterization and evaluation of the samples from Fig. 5 will be discussed in a subsequent section. Finally, in addition to the ED curves, the kinetic response for strong electrostatic adsorption (SEA) of $PtCl_6^{2-}$ on the carbon support is also shown in Fig. 5. The pH of the ED bath (9.0) was maintained above the PZC of the carbon support (pH 3.4) to prevent unwanted electrostatic adsorption of $PtCl_6^{2-}$; the amount of $PtCl_6^{2-}$ in the bath remained essentially constant for 50 min, confirming that no $PtCl_6^{2-}$ was deposited on the carbon support during ED and that Pt had been deposited only on metal (initially Pd, and then Pt) surfaces.

The data in Fig. 5 also suggest that the rate and extent of $PtCl_6^{2-}$ may depend on the instantaneous concentration of N_2H_4, which is, of course, a function of pumping speed. The effect of pumping speed of 1.39×10^{-2} M N_2H_4 on deposition of $PtCl_6^{2-}$ to give up to 11.7 wt% Pt is shown in Fig. 6. Pumping speeds ranged from 0.50 mL/min for 100 min to 1.67 mL/min for 30 min, and the initial concentration of $PtCl_6^{2-}$ was constant at 6.96×10^{-4} M. For pumping speeds less than 1.25 mL/min, the extents of deposition were much lower. This is most likely linked to the highly non-selective decomposition of N_2H_4; in basic solutions and in the presence of Group VIII metals, oxidation of N_2H_4 forms copious amounts of non-reactive H_2 (vigorous bubbling of H_2 evolution) as opposed to active, reducing species such as adsorbed H^- on the Pd or Pt metal surfaces [37,38]. A minimum threshold concentration of N_2H_4 to offset the more facile and non-reducing H_2 formation appears to be required to provide a critical concentration of active reducing species. Only at the beginning of the ED process is the product of ($PtCl_6^{2-}$ × active N_2H_4) high enough to facilitate the ED reaction. However, at pumping rates of 1.67 mL/min and 1.25 mL/min, the $PtCl_6^{2-}$ in the bath was essentially and completely reduced at 20 min and 30 min, respectively, indicating that deposition rates can be controlled above a critical concentration of N_2H_4.

3.3. Characterization of Pt-Pd/C catalysts

The surface site concentrations of electrolessly-deposited Pt and residual, exposed Pd sites were determined by using a H_2—O_2 titration method which has been previously described by Boudart et al. [35]. The cumulative H_2 uptakes and active site concentrations are reported in Table 1. Titrations were conducted for samples "as prepared", that is, after *in situ* reduction for 2 h in flowing 10% H_2/balance Ar at 200 °C in the 2920 chemisorption analyzer and also after *in situ* post-treatment of the same sample in a flow of

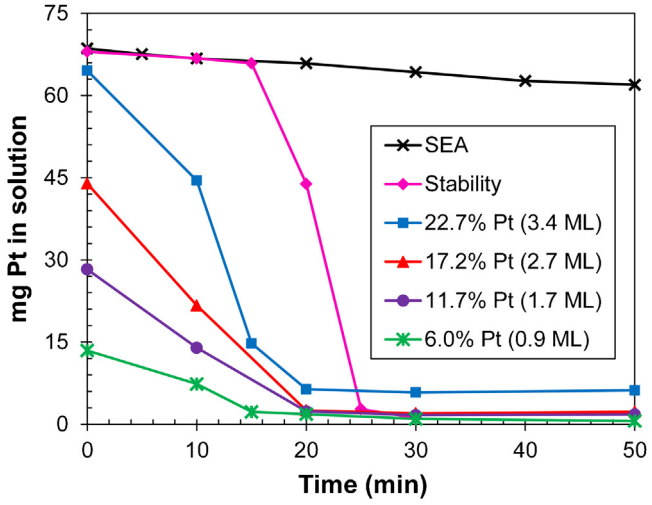

Fig. 5. Time-dependent ED profiles for various coverages of Pt on 30 wt% Pd/C at pH 9.0 with $[N_2H_4]/[PtCl_6^{2}]/[EN] = 5/1/2$ at 30 °C. N_2H_4 was pumped into ED bath for 30 min with pumping rate of 1.67 mL/min. $PtCl_6^{2-}$ concentrations remaining in bath were determined by ICP analysis.

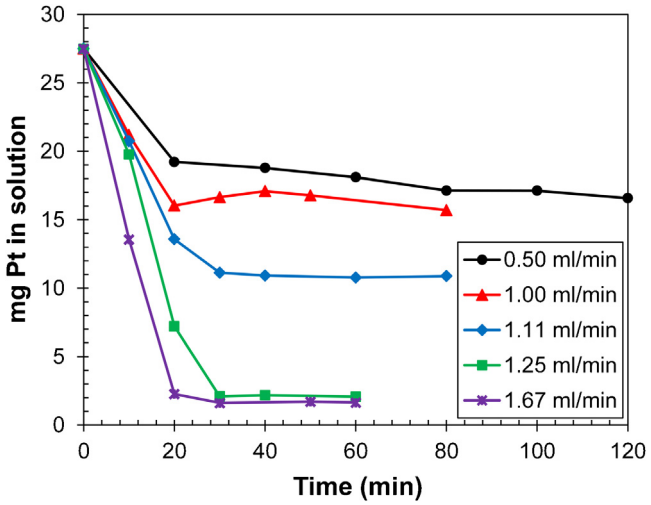

Fig. 6. Time dependent ED profiles at various N_2H_4 pumping rates. (●) 0.50 mL/min for 100 min, (▲) 1.00 mL/min for 50 min, (♦) 1.11 mL/min for 45 min, (■) 1.25 mL/min for 40 min and (×) 1.67 mL/min for 30 min.

Table 1
Cumulative H_2 uptake and active site concentrations of the catalysts from chemisorption analysis.

wt% Pt	H_2 uptake, cc(STP)H_2/g cat			Active site concentrations, site/g cat		
	As prepared	Post treat	Change %	As prepared	Post treat	Change %
0.0	11.90	11.95	0.42	2.13×10^{20}	2.14×10^{20}	0.47
6.0 (0.9 ML)	7.35	11.90	61.9	1.32×10^{20}	2.13×10^{20}	61.4
11.7 (1.7 ML)	7.93	11.84	49.3	1.42×10^{20}	2.12×10^{20}	49.3
17.2 (2.7 ML)	7.80	11.80	51.3	1.40×10^{20}	2.12×10^{20}	51.4
22.7 (3.4 ML)	7.80	10.93	40.1	1.40×10^{20}	1.96×10^{20}	40.0

10% O_2/balance He at 260 °C for 2 h, followed by reduction in flowing 10% H_2/balance Ar at 200 °C for 2 h. The post-treatment in 10% O_2 was conducted since earlier work [41] had indicated that after electroless deposition, carbon-supported metal catalysts became decorated by carbonaceous deposits from either the ED process or migration of the carbon support (in the aqueous medium) onto the surface of the metal. Similar decreases in metal surface area due to surface residues have also been reported by Datye et al. [44] for supported Pd and Pt catalysts. This carbon residue was reactive in the presence of the catalytic metal surface and catalyst-assisted oxidation of the carbon residue occurred at temperatures between 150 and 260 °C. The almost-identical chemisorption results in Table 1 for 30 wt% Pd/C indicate that the marked decreases in H_2 uptake for the samples after ED is due to organic residue on the Pt surface following electroless deposition [41,45]. For all Pt-Pd/C samples, the concentrations of active Pt (and uncovered Pd) surface sites after ED were 40–60% lower before the calcination post-treatments. Interestingly, H_2 uptake values and active site concentrations of the samples after ED and post-treatment were very similar and consistent with formation of thin Pt shells over a Pd core. Since diameters and surface areas of the controlled thickness Pt shells (~1–3 ML) on a Pd core should not differ substantially from that of the Pd core, the concentration of active Pt sites should be similar, particularly if ED occurred in a uniform manner for all particles. Indeed, the concentration of Pd surface sites for 30 wt% Pd/C (2.14×10^{20} sites/g cat) was virtually identical to the surface site concentrations for 0.9, 1.7, and 2.7 ML Pt coverages. Only for the case of 3.4 ML Pt was site concentration lowered only slightly at 1.96×10^{20} sites/g cat. Just as importantly from a perspective of preparation of all carbon-supported catalysts, these results suggest that organic residues from liquid phase reducing agents or creep of carbon support may lower surface concentrations of active metal sites. Metal-assisted, catalytic oxidation (Pt, in this case) of these residues, however, provides a facile way to remove these residues. It also calls into question whether this problem may exist for other families of carbon-supported metal catalysts that use organic reducing agents to reduce metal salt precursors.

HAADF STEM analysis was conducted for all of the catalysts containing various coverages of Pt on 30 wt% Pd/C but the 3.4 ML Pt sample and selected results are shown in Fig. 7. Fig. 7a shows the dispersed Pd particles on the support with an average particle size between 5 and 6 nm. Fig. 7b, c and d show the catalysts with 0.9, 1.7 and 2.7 ML Pt on 30 wt% Pd/C, respectively. HAADF-imaged particles contained both Pt and Pd and were all approximately 5–7 nm in size. It is not possible from either the H_2 titration values or the STEM images to determine whether the coverage of Pt on Pd is uniform for all particles at a given Pt coverage. It is likely there is some variation in Pt coverage, since both Pd (catalytic) and Pt (auto-catalytic) can activate the N_2H_4 reducing agent; only if the rates of deposition are equal for all surface sites could the coverages be uniform. Rather, it is likely there is some distribution of coverage among different particles. Analysis of many particles (approximately 50 images for each sample) for each Pt coverage, however, did show that all Pd particles had some coverage of Pt and that the coverages were rather similar. This mode of Z-contrast imaging gave both bright and dark portions for each particle in the focal plane. The darker region in the inside of the particles, indicates the presence of Pd, the lower atomic weight species. The darker core is surrounded by a brighter shell, corresponding to the Pt that was electrolessly deposited on the Pd core. The composition of the core-shell particles is confirmed by line scan EDS and the results are shown in Fig. 8.

Chemical analysis of the particles by EDS reveals the presence of platinum and palladium. The line profiles across the particle (Fig. 8a) confirm that both elements are associated with the particle. In Fig. 8c and d, the EDS line scan for Pt shows the concentration profile of Pt on the particle was highest at the edges of the particle and lower in the middle. For Pd it was the opposite; the concentration of Pd was lowest at the edges and highest in the middle. These results confirm formation of core-shell particles with Pt as discrete shells and Pd cores.

3.4. Catalyst evaluation

CV measurements were carried out in N_2-purged 0.1 M $HClO_4$ solutions at 50 mV/s. ORR polarization curves were recorded positively at a sweep rate of 10 mV/s in O_2-saturated 0.1 M $HClO_4$ at 400, 900, 1600 and 2500 rpm. The kinetic current of the catalyst (i_k) and specific activity (SA) are calculated from the mass-transport correction from rotating disc electrodes [5]. Specific activity is a turnover number and represents the current generating ability of individual Pt surface sites. For non-structure sensitive electrochemical reactions, the SA values should remain constant for all Pt surfaces.

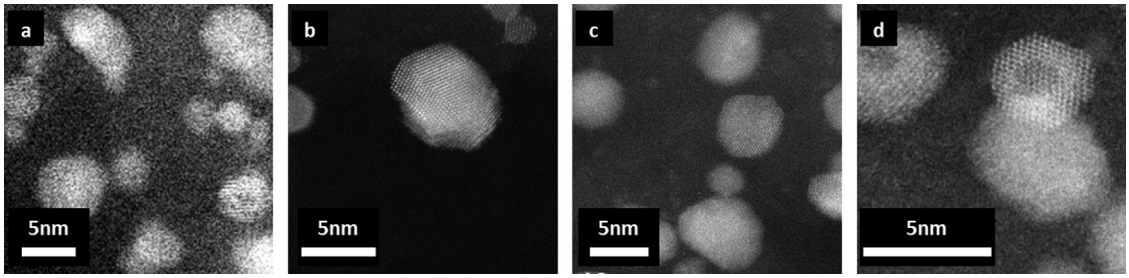

Fig. 7. HAADF images of various Pt coverages on 30 wt% Pd/C. (a) 30 wt% Pd/C base catalyst. (b) 0.9 ML Pt on 30 wt% Pd/C. (c) 1.7 ML Pt on 30 wt% Pd/C. and (d) 2.7 ML Pt on 30 wt% Pd/C.

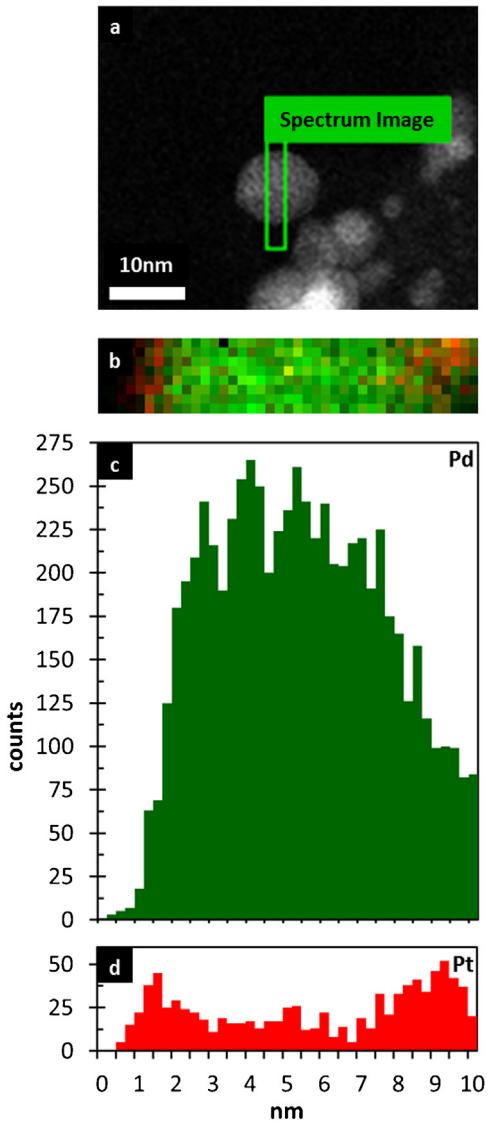

Fig. 8. HAADF image of 2.7 ML Pt on 30 wt% Pd/C and the associated EDS map and line scans; red color at the edges of the line scan represents Pt and green color in the center represents Pd. (a) HAADF image and section of particle analyzed by EDS. (b) EDS sectional elemental map. (c) EDS line scan of Pt. (d) EDS line scan of Pd. (For interpretation of the references to color in this figure legend, the reader is referred to the web version of this article.)

Table 2
Details of electrochemical activities of catalysts with different Pt coverages. Catalyst denoted as 50.5 wt% Pt/C was furnished by outside supplier and is shown for comparison.

Sample	wt loading %		MA	ECSA	SA
	Pt	Pd	(A/g-Pt)	(m^2 Pt surf/g Pt)	($\mu A/cm^2$ Pt surf)
30 wt% Pd/C	0	29.8	N/A	N/A	N/A
50.5 wt% Pt/C	50.5	0	183	58	316
0.9 ML Pt	6.0	28.2	329	211	156
1.7 ML Pt	11.0	26.7	218	109	200
2.7 ML Pt	17.0	25.0	228	72	317
3.4 ML Pt	21.6	23.5	157	87	180

The electrochemical surface area (ECSA) was calculated from the integrated hydrogen adsorption area of cyclic voltammograms and defines the concentration of Pt surface sites per gram of Pt; this is the same as the term "dispersion" used in conventional catalysis, which would be defined as the number of Pt surface atoms/total number of Pt atoms. From the above, the mass activity (MA), which is the product of SA and ECSA, can be calculated. This is the term most often used to describe the efficiency of Pt utilization in a fuel cell, since it relates performance to Pt costs. These parameters as a function of Pt coverage on Pd are shown in Fig. 9 and summarized in Table 2.

Also included in Table 2 are results for a commercial Pt/C sample that contains 50.5 wt% Pt. As seen from Fig. 9, mass activities increase as Pt shell thickness decreases, consistent with more efficient use of Pt as thickness approaches one ML of Pt. For multi-layer Pt coverages, the bulk Pt does not contribute to the ORR reaction and MA decreases. ECSA follows the same general trend, again since only the uppermost Pt layer contributes to the ORR surface reaction. Assuming there no effects of Pt in underlying near-surface layers, the highest ECSA and MA values should exist for single monolayer coverages of Pt. However, if multilayers of Pt are needed to offset potential negative effects of the core metal on a single monolayer shell of Pt [46], it is important to prepare controlled multilayers of Pt. For monometallic Pt particles, complete exposure of all Pt atoms can only be achieved for particles $\leq$1 nm in diameter, which are very difficult to prepare and are unstable during fuel cell operation [5]. Thus, a very effective way to achieve only surface Pt atoms is to deposit only a single ML thickness of Pt on a stable core metal. In this case, we have shown that ~1 ML Pt can be deposited on Pd by electroless deposition. The values for SA in Table 2 for 0.9, 1.7, and 3.4 ML Pt coverages are rather similar at 156, 200, and 180 $\mu A/cm^2$ Pt surf, respectively, suggesting no sensitivity to shell thickness. Surprisingly, the specific activity (SA) of 317 $\mu A/cm^2$ Pt surf in Fig. 9 is highest for the sample with 2.7 ML shell thickness; we have no explanation for this unusually high value, but from previous work [47] believe it may be due to an error in controlling the amount of material on the glassy carbon surface of the RDE. However, the

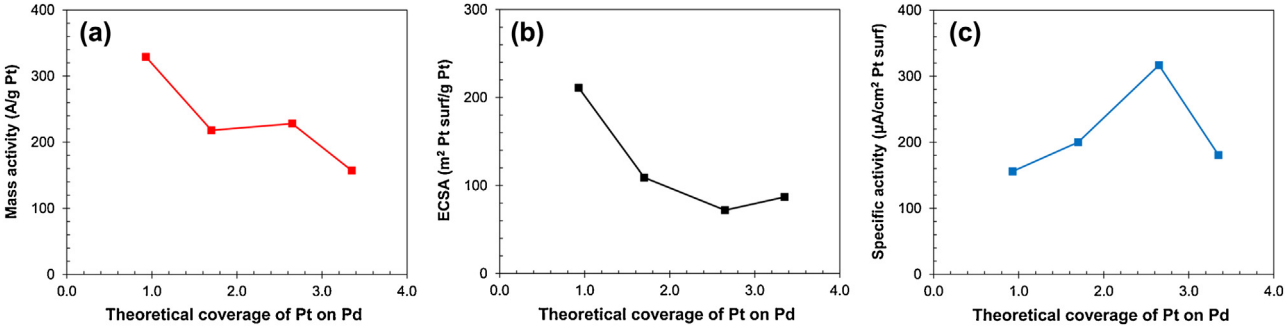

Fig. 9. Electrochemical evaluation using RDE method for Pd core-Pt shell samples. (a) Mass activity. (b) ECSA. (c) Specific activity. RDE was done in O_2-saturated 0.1 M $HClO_4$ at 27 °C and 400, 900, 1600 and 2500 rpm. Scan rate was 10 mV/s and current measured at 0.9 V vs RHE.

SA of the other Pt coverages are quite consistent between 156 and 200 μA/cm^2 Pt surf. One of the problems with examination of conventional Pt catalysts with smaller Pt particle sizes for greater Pt efficiency is the inherent instability of small Pt particle sizes with respect to sintering. In previous work, however, we have shown that Pt layers deposited on small Pd particles did not undergo sintering even after accelerated aging tests [9]. Thus, the Pd core-Pt shell structures of this study provide both a way to maximize Pt efficiency and maintain particle sizes.

More importantly, the results in Table 2 show that as the Pt weight loading increases (thicker Pt shells), the mass activities decrease. By comparison, the commercial sample containing 50.5 wt% Pt had a mass activity of 183 A/g Pt, considerably lower than the values for all Pt shell-Pd core samples.

For comparison to the results of others, the mass activity for 0.9 ML Pt coverage was 329 A/g Pt compared with the value of 190 A/g Pt for a Pd core-Pt shell/C sample prepared by Zhang et al. [48]. Gasteiger et al. [5] has also reported MA values of 64–160 A/g Pt for a series of Pt/C catalysts with Pt loadings ranging from 20 to 46 wt%. In this study, the MA of 329 A/g Pt is 77% of the value of 440 A/g Pt mandated by DOE for 2017 [49]. The initial results in this study suggest that electroless deposition may be a promising method to achieve the goals set by DOE and that deposition of Pt on smaller Pd particles as well as on different core metals such may permit the formation of Pt-containing surface sites that have higher specific activities due to structural and/or electronic interactions between Pt and the core metal. In a more general sense, we have shown that electroless deposition is a viable and predictive method for preparation of controlled-thickness metal shells on different metal cores.

4. Conclusions

A method of semi-continuous electroless deposition has been developed for the deposition of high weight loadings of Pt on 30 wt% Pd/C. The deposition of Pt on Pd readily occurred in an aqueous bath containing a reducible metal salt ($PtCl_6^{2-}$), reducing agent (hydrazine) and stabilizer (ethylenediamine). Three possible deposition reactions of Pt can take place in the ED bath; the strong electrostatic adsorption of $PtCl_6^{2-}$ on the carbon support, the thermal reduction of $PtCl_6^{2-}$ with hydrazine in the ED bath and the electroless deposition of Pt on Pd, which is the desirable reaction. To avoid electrostatic adsorption of $PtCl_6^{2-}$, the pH of the bath must be maintained higher than the PZC of the carbon support to generate a negatively-charged carbon surface; in this work, the bath was controlled at pH 9.0. Bath stability was maintained by limiting the concentration of N_2H_4 in the bath to prevent thermal reduction of $PtCl_6^{2-}$ to form Pt^0 particles. The concentration of N_2H_4 was controlled by pumping N_2H_4 solutions at various pumping rates into the ED bath. With this methodology, bimetallic Pt-Pd particles with Pt loadings of 6.0, 11.7, 17.2, and 22.7 wt% were selectively deposited on 30 wt% Pd particles. The structures of the catalysts were revealed by STEM and EDS as variable thickness Pt shell with Pd cores. Pt loadings of 6.0, 11.7, 17.2, and 22.7 wt% corresponding to Pt shells with 0.9, 1.7, 2.7, and 3.4 monolayers on Pd were prepared. The ability to reproducibly prepare controlled-thickness Pt shells on Pd (or other metals) core particles provides the means to utilize the more expensive Pt component very efficiently since the Pt-catalyzed reactions in the PEM fuel cell are surface reactions; the interior bulk atoms are not directly involved in catalysis. With the development of semi-continuous ED, preparation of large quantities of material becomes feasible. Finally, evaluation of the catalysts to ORR has been conducted and as expected, the catalyst with the 0.9 ML shell of Pt exhibited the highest mass activity of 329 A/g-Pt; mass activities decreased as Pt shell thickness increased.

Acknowledgements

We would like to thank Tetsuo Kawamura and Yusuke Itoh, Toyota Motor Corporation, for their valuable discussions and for helping with preparation of the manuscript and to Toyota Motor Company for supporting a portion of this work.

References

[1] O.T. Holton, J.W. Stevenson, Platinum Met. Rev. 57 (2013) 259–271.
[2] A.J. Appleby, J. Electroanal. Chem. 357 (1993) 117–179.
[3] H.A. Gasteiger, N.M. Marković, Science 324 (2009) 48–49.
[4] J. Greeley, I.E.L. Stephens, A.S. Bondarenko, T.P. Johansson, H.A. Hansen, T.F. Jaramillo, J. Rossmeisl, I. Chorkendorff, J.K. Nørskov, Nat. Chem. 1 (2009) 552–556.
[5] H.A. Gasteiger, S.S. Kocha, B. Sompalli, F.T. Wagner, Appl. Catal. B 56 (2005) 9–35.
[6] E. Antolini, J.R.C. Salgado, M.J. Giz, E.R. Gonzalez, Int. J. Hydrogen Energy 30 (2005) 1213–1220.
[7] T. Toda, H. Igarashi, H. Uchida, M. Watanabe, J. Electrochem. Soc. 146 (1999) 3750–3756.
[8] N.M. Sánchez-Padilla, D. Morales-Acosta, M.D. Morales-Acosta, S.M. Montemayor, F.J. Rodríguez-Varela, Int. J. Hydrogen Energy 39 (2014) 16706–16714.
[9] M. Ohashi, K.D. Beard, S. Ma, D.A. Blom, J. St-Pierre, J.W. Van Zee, J.R. Monnier, Electrochim. Acta 55 (2010) 7376–7384.
[10] W. Diao, J.M.M. Tengco, J.R. Regalbuto, J.R. Monnier, ACS Catal. 5 (2015) 5123–5134.
[11] K.D. Beard, D. Borrelli, A.M. Cramer, D. Blom, J.W. Van Zee, J.R. Monnier, ACS Nano 3 (2009) 2841–2853.
[12] K.D. Beard, J.W. Van Zee, J.R. Monnier, Appl. Catal. B 88 (2009) 185–193.
[13] J.K. Nørskov, J. Rossmeisl, A. Logadottir, L. Lindqvist, J.R. Kitchin, T. Bligaard, H. Jónsson, J. Phys. Chem. B 108 (2004) 17886–17892.
[14] R. Lin, C. Cao, T. Zhao, Z. Huang, B. Li, A. Wieckowski, J. Ma, J. Power Sources 223 (2013) 190–198.
[15] Z. Wei, H. Guo, Z. Tang, J. Power Sources 62 (1996) 233–236.
[16] G. Ertl, H. Knozinger, J. Weitkamp (Eds.), Handbook of Heterogeneous Catalysis, vol. 1, VCH Verlag Sgesellschaft, Weinheim, 1997 (pp. 13, 35–38, 191–195, 257–261, 365–367).
[17] M.B. Vukmirovic, J. Zhang, K. Sasaki, A.U. Nilekar, F. Uribe, M. Mavrikakis, R.R. Adzic, Electrochim. Acta 52 (2007) 2257–2263.
[18] S.R. Brankovic, J.X. Wang, R.R. Adžić, Surf. Sci. 474 (2001) L173–L179.
[19] K. Sasaki, J.X. Wang, H. Naohara, N. Marinkovic, K. More, H. Inada, R.R. Adzic, Electrochim. Acta 55 (2010) 2645–2652.
[20] J.L. Reyes-Rodríguez, F. Godínez-Salomón, M.A. Leyva, O. Solorza-Feria, Int. J. Hydrogen Energy 38 (2013) 12634–12639.
[21] L. Gan, C. Cui, M. Heggen, F. Dionigi, S. Rudi, P. Strasser, Science 346 (2014) 1502–1506.
[22] R. Feng, M. Li, J. Liu, Colloids Surf. A 406 (2012) 6–12.
[23] B. Habibi, S. Ghaderi, Int. J. Hydrogen Energy 40 (2015) 5115–5125.
[24] G. Topalov, G. Ganske, E. Lefterova, U. Schnakenberg, E. Slavcheva, Int. J. Hydrogen Energy 36 (2011) 15437–15445.
[25] Y. Xu, Y. Dong, J. Shi, M. Xu, Z. Zhang, X. Yang, Catal. Commun. 13 (2011) 54–58.
[26] G. Bahmanrokh, M. Hashim, K.A. Matori, M. Navasery, N. Soltani, P. Vaziri, S. Kanagesan, R. Sabbaghizadeh, M.S. Ezzad Shafie, J. Appl. Phys. 116 (2014) 093907.
[27] H. Zhang, Y. Yin, Y. Hu, C. Li, P. Wu, S. Wei, C. Cai, J. Phys. Chem. C 114 (2010) 11861–11867.
[28] Y. Yamada, K. Miyamoto, T. Hayashi, Y. Iijima, N. Todoroki, T. Wadayama, Surf. Sci. 607 (2013) 54–60.
[29] C.A. Cortés-Escobedo, R.d.G. González-Huerta, A.M. Bolarín-Miró, F. Sánchez de Jesús, Q. Zhu, S.E. Canton, K. Suarez-Alcantara, M. Tufiño-Velazquez, Int. J. Hydrogen Energy 39 (2014) 16722–16730.
[30] Y. Zhang, W. Diao, C.T. Williams, J.R. Monnier, Appl. Catal. A 469 (2014) 419–426.
[31] K.D. Beard, M.T. Schaal, J.W. Van Zee, J.R. Monnier, Appl. Catal. B 72 (2007) 262–271.
[32] R.P. Galhenage, K. Xie, W. Diao, J.M.M. Tengco, G.S. Seuser, J.R. Monnier, D.A. Chen, Phys. Chem. Chem. Phys. 17 (2015) 28354–28363.
[33] T.R. Garrick, W. Diao, J.M. Tengco, J. Monnier, J.W. Weidner, ECS Trans. 53 (2013) 79–84.
[34] E.J. O'Sullivan, Adv. Electrochem. Sci. Eng. 7 (2001) 225–271.
[35] J.E. Benson, H.S. Hwang, M. Boudart, J. Catal. 30 (1973) 146–153.
[36] Y. Zhang, W. Diao, J.R. Monnier, C.T. Williams, Catal. Sci. Technol. 5 (2015) 4123–4132.
[37] I. Ohno, O. Wakabayashi, S. Haruyama, J. Electrochem. Soc. 132 (1985) 2323–2330.
[38] S. Haruyama, I. Ohno, Proc. Electrochem. Soc. 88 (1988) 20–36.
[39] S.S. Djokić, Modern Aspects of Electrochemistry, in: B.E. Conway, R.E. White (Eds.), Springer, US, 2002, pp. 51–133.
[40] I. Ohno, Mater. Sci. Eng. A 146 (1991) 33–49.

[41] J.M.M. Tengco, Y.K. Lugo-José, J.R. Monnier, J.R. Regalbuto, Catal. Today 246 (2015) 9–14.
[42] A. Henglein, B.G. Ershov, M. Malow, J. Phys. Chem. 99 (1995) 14129–14136.
[43] D.L. Swihart, W.R. Mason, Inorg. Chem. 9 (1970) 1749–1757.
[44] A.K. Datye, Q. Xu, K.C. Kharas, J.M. McCarty, Catal. Today 111 (2006) 59–67.
[45] J.R. Regalbuto, Catalyst Preparation: Science and Engineering, in: J.R. Regalbuto (Ed.), CRC Press, Boca Raton, 2006, pp. 297–318.
[46] R.R. Adzic, J. Zhang, K. Sasaki, M.B. Vukmirovic, M. Shao, J.X. Wang, A.U. Nilekar, M. Mavrikakis, J.A. Valerio, F. Uribe, Top. Catal. 46 (2007) 249–262.
[47] K. Punyawudho, D.A. Blom, J.W. Van Zee, J.R. Monnier, Electrochim. Acta 55 (2010) 5349.
[48] G. Zhang, Z.-G. Shao, W. Lu, F. Xie, H. Xiao, X. Qin, B. Yi, Appl. Catal. B 132–133 (2013) 183–194.
[49] M.K. Debe, Nature 486 (2012) 43–51.